

Multispectral Imaging using Sinusoid Pattern and Modern Spectrum Estimation

Cui Ma

Shenzhen Institutes of Advanced Technology, Chinese Academy of Sciences
Shenzhen, Guangdong, China
Shenzhen College of Advanced Technology, University of Chinese Academy of Sciences
cui.ma@siat.ac.cn

Received February, 2018; revised March, 2018

ABSTRACT. *Recently, we have introduced a Digital Micro-mirror Device (DMD) based multispectral imaging using Fourier spectrum. The sinusoid pattern is used for encoding the pixel spectrum and the Inverse Fourier Transform (IFT) decodes the spectrum. In this paper, an enhanced multispectral imaging is introduced. On one hand, the spatial resolution is improved considering the difference between CCD pixel and DMD coding pixel size. On the other hand, the modern spectrum estimation method is applied to improve the reconstructed spectral curve using limited coefficients. The experiment shows that this method performs well. The decoded images have the maximal spatial resolution which is the same as CCD detected image without pixel merging. And the modern spectrum estimation method is better than Inverse Fourier Transform (IFT) using the same number of Fourier coefficients.*

Keywords: Multispectral imaging, Fourier transform, Modern spectrum estimation

1. **Introduction.** Multispectral imaging combines the spectrometer and imaging. It includes two-dimensional spatial information and one-dimensional spectral information. It is a 3D data set and can be viewed as a datacube. It is widely used in remote sensing, biology, etc. There have been many methods for spectral imaging. Mainly, it can be divided into wavelength-scan method, spatial-scan method, time-scan method, the non-scanning method which measures the spatial and spectral simultaneously [1, 2]. Fourier spectral imaging [3, 4] and Hadamard transform spectral imaging (HTSI) [5, 6] are both time-scan method [1]. They are multiplex measurement and suitable for weak signals. Fourier spectral imaging is usually based on interferometer [3] or sinusoidal filters [7, 8]. The Fourier Transform is used to obtain the spectrum in wavenumber domain. HTSI is based on the Hadamard coding pattern. The Hadamard transform is used to decode the spectrum in wavelength domain.

In this paper, the multispectral imaging system has the similar optical structure of HTSI, but realizes the Fourier transform. The sinusoid pattern [9, 10] is used for encoding the pixel spectrum and transforms the spectrum into Fourier domain. Our research has validated that the DMD is feasible to generate different periods of sinusoid patterns to implement spectral imaging [11]. But it has some limitations. First, there is the pixel matching problem for DMD coding pixel and CCD pixel. Usually, CCD pixels should be merged to match the coding pixel size. This will decrease the spatial resolution. Second, the generated sinusoid pattern is the sampled value of the ideal sinusoidal pattern using DMD coding pixel. It has large difference between generated sinusoidal pattern and ideal

pattern when sinusoidal period is small. Therefore, a limited Fourier coefficients are used and avoid the error of high-order Fourier coefficients. In this paper, the CCD pixels are not merged to get the maximal spatial resolution. Besides, instead of setting the undetected coefficients to zeros, the modern spectrum estimation method [12] is introduced to estimate the undetected values. It will improve the decoded spectrum using limited coefficients.

The paper is organized as follows. Part 2 is the theory, including the pixel spectrum encoding, decoding and sinusoid pattern generation. Part 3 shows a simulation. Part 4 gives the experimental results. And finally, part 5 is the conclusions.

2. Theory.

2.1. Spectrum encoding using sinusoid pattern. Fig.1 gives the optical schematic of multispectral imaging system. It is similar to the HTSI system. The first grating disperses the object light to a serial of wavebands. Then, coding pattern encodes the dispersed spectrum. Finally, the second grating recombines the wavebands and CCD detects the encoded image. Suppose the spectrum is dispersed along n axis and forms K wavebands ($\lambda_r, r = 0, 1, \dots, K - 1$). The datacube is denoted as $\{I(m, n, \lambda_r)\}$.

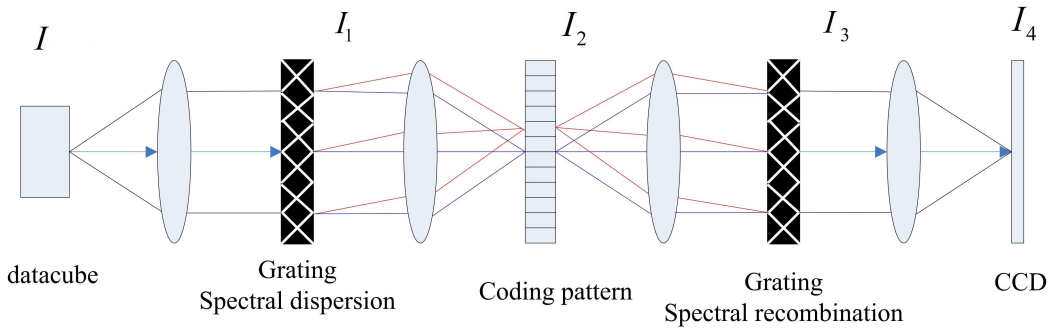


FIGURE 1. Optical schematic of multispectral imaging

Assuming the grating is linear dispersion, the spectral intensity after grating with linear dispersion α is then

$$I_1(m, n, \lambda_r) = I(m, n + \alpha(\lambda_r - \lambda_0), \lambda_r) \quad (1)$$

Immediately after the coding pattern, the spectral intensity is given by:

$$I_2(m, n, \lambda_r) = T(m, n)I_1(m, n, \lambda_r) \quad (2)$$

where $T(m, n)$ is the transmission function imposed by coding pattern. After a set of imaging optics and the second grating, the spectral density is:

$$I_3(m, n, \lambda_r) = I_2(m, n - \alpha(\lambda_r - \lambda_0), \lambda_r) = T(m, n - \alpha(\lambda_r - \lambda_0))I(m, n, \lambda_r) \quad (3)$$

This indicates that the coding pattern is shifted with wavelength for different spectral band image. However, the CCD detector is wavelength-insensitive. It gathers the spectral images of different wavelength, illustrated in Eq.(4).

$$I_4(m, n) = \sum_{r=0}^{K-1} T(m, n - \alpha(\lambda_r - \lambda_0))I(m, n, \lambda_r) \quad (4)$$

Different with HTSI, the sinusoid pattern is used for coding in this paper. The patterns are generated by Digital Micro-mirror Device (DMD). The Fig. 2(a) is Hadamard patterns used for HTSI. They are 0-1 values. Fig. 2(b) is sinusoid patterns which are gray values.

Varying the harmonic order k of sinusoid pattern, we can get a series of encoded spectrum. The encoded spectrum is in Fourier domain and can be decoded using Inverse Fourier Transform (IFT). Fig.3 shows the process of encoding and decoding.

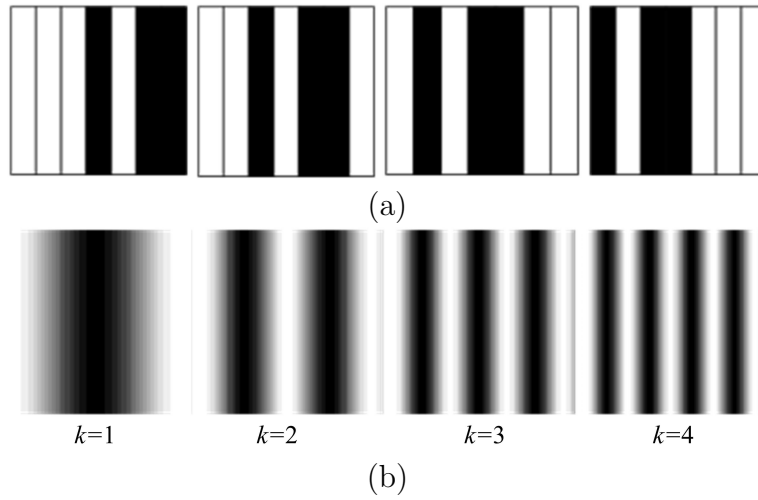


FIGURE 2. (a)Hadamard coding patterns, (b)sinusoid patterns

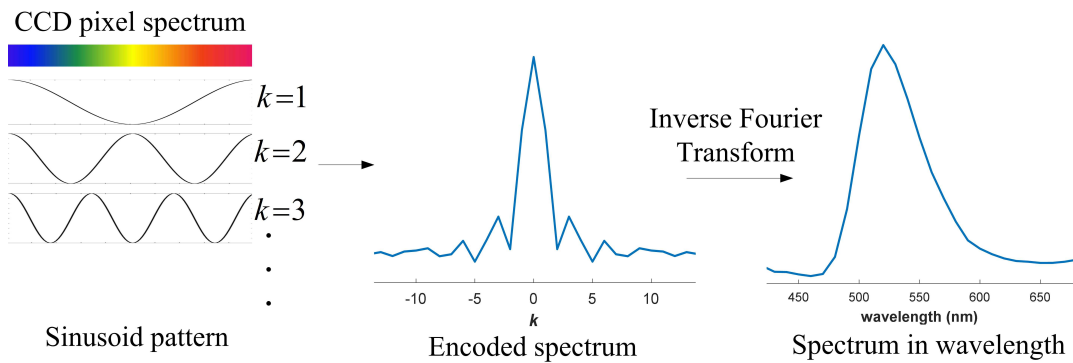


FIGURE 3. Illustration of the spectrum encoded by sinusoid pattern and decoded by IFT

For pixel (m, n) on the CCD, the encoded spectrum is given by:

$$I_4(m, n) = \sum_{r=0}^{K-1} \cos\left(\frac{2\pi kr}{K} + \varphi\right) \cdot I(m, n, \lambda_r) \tag{5}$$

where φ is the initial phase; $k = 0, 1, \dots, K - 1$ is the harmonic order; $r = 0, 1, \dots, K - 1$ is used to index the wavebands. The Fourier coefficient $P(m, n, k)$ is obtained by combining the sinusoidal patterns with phase $\varphi = 0$ and $\varphi = \pi/2$, expressed by:

$$P(m, n, k) = \sum_{r=0}^{K-1} I(m, n, \lambda_r) \cdot \exp\left(\frac{-i2\pi kr}{K}\right) \tag{6}$$

For pixels with different n , the coding pattern of its spectrum has a shift Δn . The shift is 1 for adjacent pixels when CCD pixel and DMD coding pixel has the same size. However, the CCD pixel size is smaller than DMD coding pixel usually. The commonly used method is merging the CCD pixels to match the DMD coding pixel size. Taking the Fig. 4 for example, one DMD coding pixel has the same size with 2 CCD pixels. When

the CCD pixels are merged, the spatial resolution will decrease. Here, the pixels are not merged and the coding pattern for every pixel is analyzed.

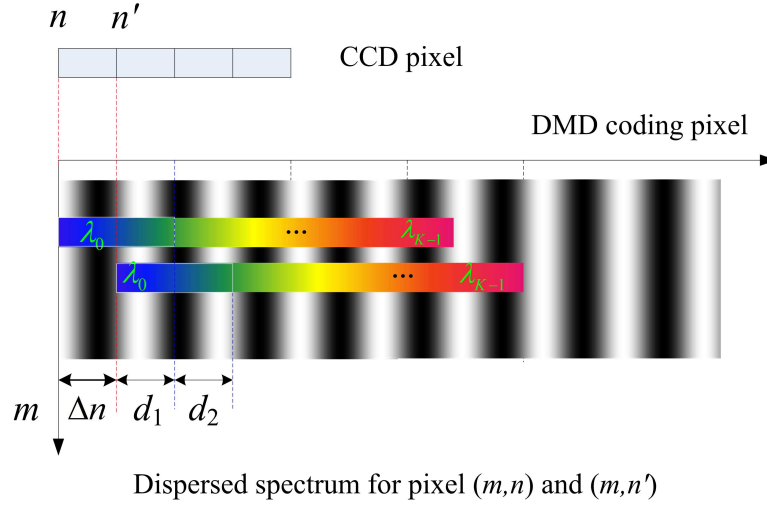


FIGURE 4. An example of the pixel mismatching and the DMD coding pixel size is double the CCD pixel. The spectrum of (m, n) is one-to-one correspondence with DMD coding pixel, but the spectrum of (m, n') has a shift and encoded by two DMD coding pixels partially

For the adjacent CCD pixel (m, n') , the wavebands are not one-to-one with DMD coding pixels. Every waveband is encoded with two neighbor coding values partially. The Eq. (5) is improved considering the pixel size scale, given by Eq. (7).

$$I_4(m, n') = \sum_{r=0}^{K-1} \left[\cos \left(\frac{2\pi kr}{K} + \varphi \right) \cdot d_1 + \cos \left(\frac{2\pi k(r+1)}{K} + \varphi \right) \cdot d_2 \right] \cdot I(m, n', \lambda_r) \quad (7)$$

where d_1 and d_2 are relevant with DMD coding pixel size and CCD pixel size.

Changing the sinusoidal pattern using different order k and looping the aforementioned procedure, a series of Fourier coefficients can be obtained. Then, the pixel spectrum can be decoded using Inverse Fast Fourier Transform (IFFT).

$$I(m, n', \lambda_r) = C \cdot F^{-1} [P(m, n', k) \cdot C_{n'}], r = 0, 1, \dots, K-1; k = 0, 1, \dots, K-1 \quad (8)$$

where $C_{n'} = \exp \left(\frac{i2\pi k}{K} \right) \cdot [d_1 + d_2 \cdot \exp \left(\frac{i2\pi k}{K} \right)]$ is a constant for pixel (m, n') and order k . C is a constant for IFFT.

Similarly, we can get the entire datacube when the spectrum of every pixel is decoded.

2.2. Decoding using modern spectrum estimation. The information of natural object is usually sparse in Fourier domain, so the signal can be compressed and only a part of Fourier coefficients are detected. When $k < K$, the rest Fourier coefficients are defaulted as zeros when using IFFT, in fact, they are not all zeros. Here, the modern spectral estimation [12] is used to improve resolution using limited measurements. AR (Auto-Regressive) is a linear prediction model that it could be employed for predicting the rest Fourier coefficients using a set of known data. The q order AR model is used.

$$P(k) = - \sum_{v=1}^q a_v P(k-v) + \omega(k) \quad (9)$$

where $P(k)$ is the random sequence, in our system it is the Fourier coefficients. $\omega(k)$ is white noise and a_k is factor. And its power spectral estimation is:

$$P_{AR}(w) = \frac{\sigma_w^2}{\left|1 + \sum_{v=1}^q a_v e^{-jwv}\right|^2} \quad (10)$$

where σ_w^2 is the variance of prediction error. The power spectrum can be estimated by calculating σ_w^2 and a_k . Burg algorithm is a useful method to calculate the parameters of AR model directly from the detected Fourier coefficients. Then, the spectrum can be reconstructed using the estimated parameters and appropriate order q .

2.3. Sinusoid pattern generation. As mentioned above, sinusoid pattern is used to encode the pixel spectrum. This is done using DMD. In general, the sinusoid pattern shall be a series of gray values. Because of the binary nature of DMD, time dithering is therefore needed to generate the gray values. The workflow is as Fig. 5. The ideal sinusoid is firstly sampled according to the DMD coding pixel size. And the gray values for every coding pixel are obtained. Then several binary values are composed to generate gray values.

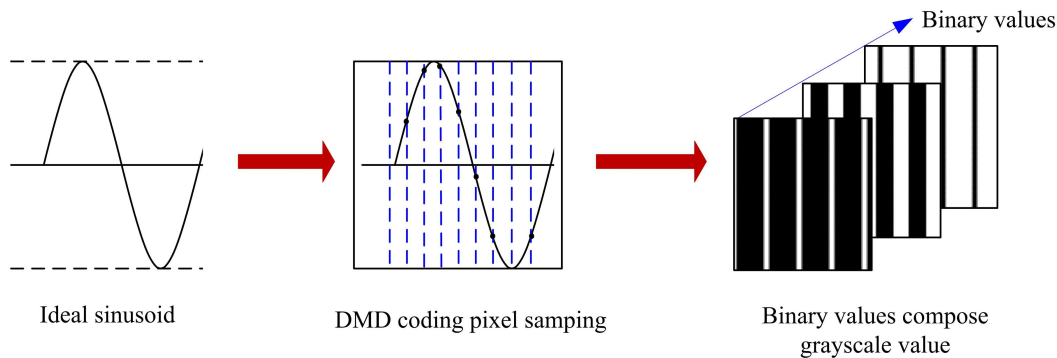


FIGURE 5. The workflow of generating DMD sinusoid pattern

There are two factors affecting the generated values. The first factor is the DMD coding pixel sampling. When k is large, the sinusoid period is small. The coding pixel sampling will not satisfy the Nyquist theory and bring errors. The Fig. 6 is an example. The sampled pattern is greatly different with ideal sinusoid pattern. The coding pattern error will bring false detection. Therefore, increasing sampling number may bring extra errors.

The second factor is the number of binary values used for composing a gray value. For example, the grayscale of the resulting pattern is composed by the $L(L = 8)$ binary values. Suppose a grayscale value 0.9, 7 binary values should be set to 1 and the other binary values are set to 0, so as to up to the nearest value $7/8$. If $L=5$, the nearest value is $4/5$ or 1 with larger difference. So, the binary number L must not be too small. The proper number L will be discussed in the simulation part.

3. Simulation. A sample set of multispectral images [13] is used for simulation. The image set includes $K = 31$ wavebands of images from 400nm to 700nm with an equal spectral spacing of 10nm.

Multispectral images are reconstructed using different number of Fourier coefficients. The mean Peak Signal to Noise Ratio (PSNR) is used to judge the similarity between the reconstructed spectral images and the original spectral images. Fig. 7 shows mean PSNR

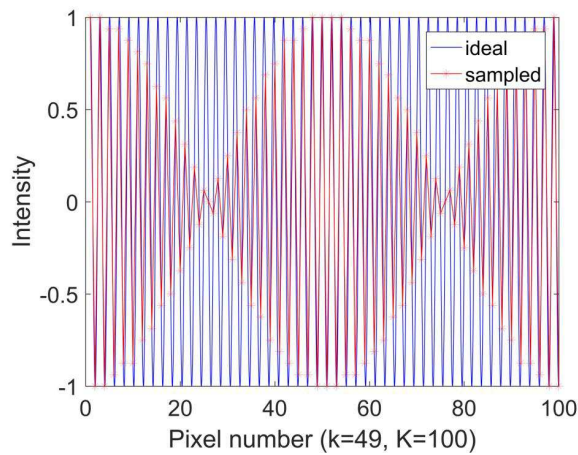


FIGURE 6. The sampled pattern with great errors under small sinusoid period(k is large)

versus coefficient number. When the number of Fourier coefficients used is larger than 5, the mean PSNR is over 30dB. It indicates the reconstructed spectral images are similar to the original images. With the increase of Fourier coefficients number, the mean PSNRs rise and then reduce. This is consistent with the analysis above. When the number of Fourier coefficients is large, it will have extra error and decrease the spatial quality. Thanks to the signal sparsity in Fourier domain, only a part of Fourier coefficients can be used for reconstruction. And the modern spectrum estimation will improve the reconstructed spectral images with limited coefficients.

Besides, the effect of binary number L is analyzed. The larger L is better, but larger L may increase measurement time. According to the Fig. 7, the $L=8$ is a proper value. To see the results clearly, Fig. 8 displays the simulation results using 5 Fourier coefficients and different number L . The reconstructed images with $L=5$ have slight strips and decrease the spatial quality. For the $L=8$, the images are almost the same as original images.

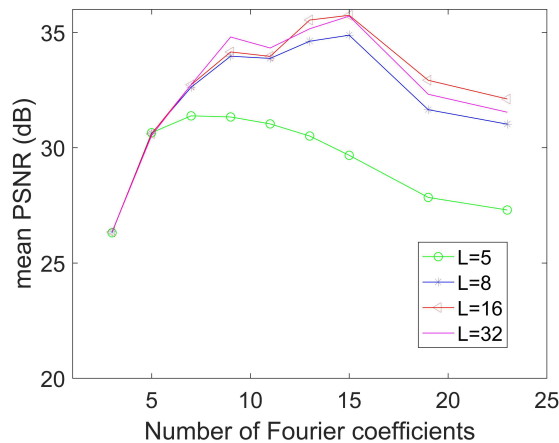


FIGURE 7. The PSNRs of reconstructed spectral images using different number of Fourier coefficients and different binary number L

4. Experiment.

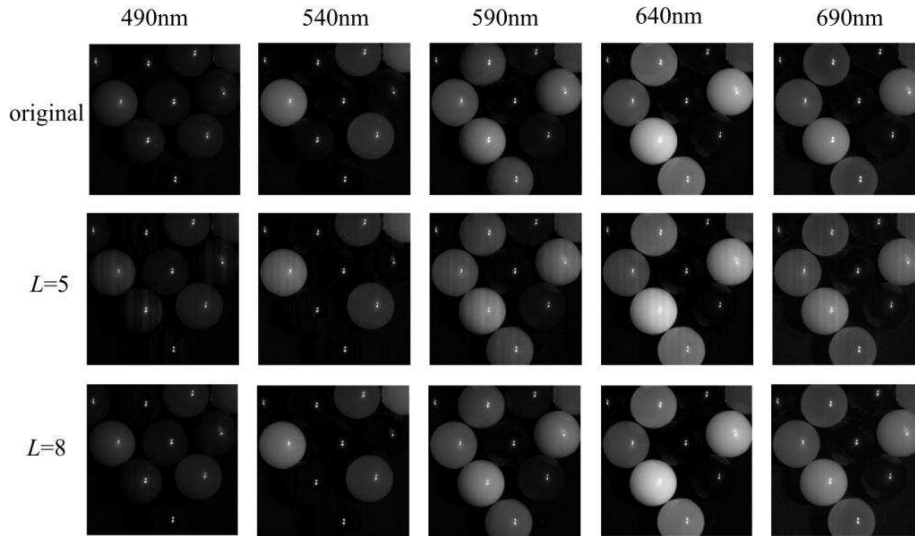


FIGURE 8. Simulation results using 5 Fourier coefficients and different number L

4.1. **Experiment setup.** To further validate our new method, an experimental testbed is built as shown in Fig. 9. The optical system is similar with HTSI. The grating 1 disperses light and DMD encodes the spectrum. Then, grating 2 recombines the dispersed spectrum. Finally, CCD detects the encoded spectral images.

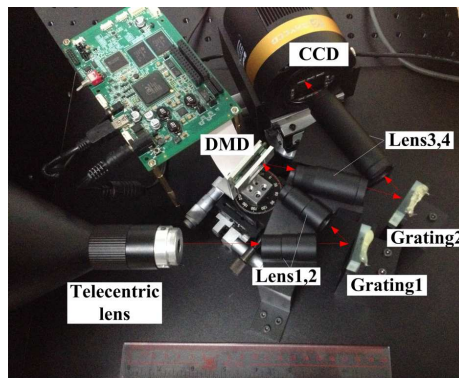


FIGURE 9. A photo of the testbed

The custom-made collimating and focusing lenses (Lens 1, 2 and Lens 3, 4) are optimized for the spectral range from 480nm to 660nm. In the experiments, the entire visible wavelength between 400 and 700nm are encoded. It covers about 93 DMD pixels and hence, the number of spectral bands K is set to 93. According to the specifications of the devices, 2 CCD pixels (QHY21, pixel size is $4.54 \times 4.54 \mu\text{m}$) are approximately equal to one DMD pixels in size (DLP4500, pixel size is equivalent to $10.8 \times 5.4 \mu\text{m}$ due to the diamond pixel configuration).

4.2. **Experiment results.** In the test, a set of digital numbers with different colors are used as shown in Fig. 10(a). Fig. 10(b) shows a selection of multispectral images reconstructed using 9 Fourier coefficients and IFFT method. The digital numbers appear in the multispectral images gradually. It indicates that the multispectral images can distinguish different colors exactly. Because the spectrum of every pixel is decoded using

Eq. (8), the reconstructed spectral images have the same spatial resolution as CCD detected image without pixel merging.

Fig. 11 shows the corresponding spectral curves. The reference spectrum are measured by a commercial spectrometer (Manufacturer: Ocean Optics, Model: USB4000). Fig. 11(a), 11(b), 11(c) and 11(d) are the spectral curves at digital number 1, 2, 4 and 5, respectively. The half-peak width of reconstructed spectrum becomes wider with the decrease of Fourier coefficients. The spectrum using 9 coefficients is better than the 5 coefficients and more similar to the reference spectrum. Besides, the spectral curves using AR algorithm with 5 coefficients are similar to the IFFT with 9 coefficients. That is, AR method improves the reconstructed spectrum when using the same number of Fourier coefficients.

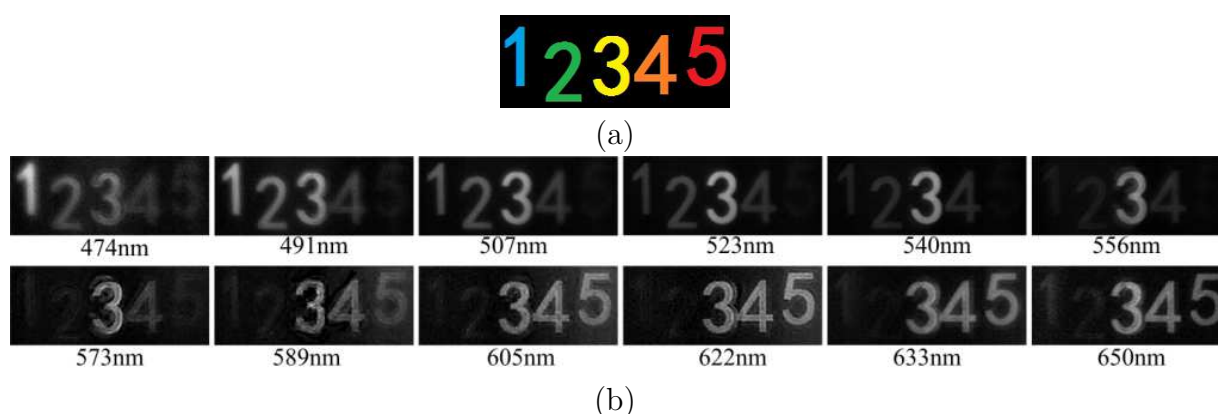


FIGURE 10. The testing results, (a) photo of the object; (b) reconstructed spectral images using 9 Fourier coefficients and IFFT

5. Conclusions. This paper introduces a multispectral imaging using sinusoid pattern and modern spectrum estimation. The sinusoid pattern is used for encoding the pixel spectrum. And modern spectrum estimation is applied to decode the spectrum using limited Fourier coefficients. The experiment shows that only a small number of Fourier coefficients can reconstruct the spectral images well and distinguish different colors. The reconstructed spectral images have the same spatial resolution as CCD detected image without pixel merging. And the spectrum is improved using modern spectrum estimation with the same number of coefficients.

Acknowledgment. This work is partially supported by Shenzhen Fundamental Research Program (JCYJ20160429191402619). The authors also gratefully acknowledge the helpful comments and suggestions of the reviewers, which have improved the presentation.

REFERENCES

- [1] Y. Garini, I. T. Young, and G. McNamara, Spectral imaging: Principles and applications *Cytometry Part A*, vol.69, no.8, pp.735C747, 2006.
- [2] A. Shay, I. Y. August, and A. Stern, Compressive and classical hyperspectral systems-a fundamental comparison, *Proc. SPIE*, vol. 9484, 948408, 2015.
- [3] T. Inoue, K. Itoh, and Y. Ichioka, Fourier-transform spectral imaging near the image plane, *Opt. Lett.*, vol.16, no.12, pp.934-936, 1991.
- [4] R. D. Alcock, and J. M. Coupland, A compact, high numerical aperture imaging Fourier transform spectrometer and its application, *Meas. Sci. Technol.*, vol.17, no.11, 2861-2868, 2006.
- [5] C. M. Wehlburg, J. C. Wehlburg, S. M. Gentry, and J. Smith, Optimization and Characterization of an Imaging Hadamard Spectrometer, *Proc. SPIE*, vol.4381, pp.506-515, 2001.

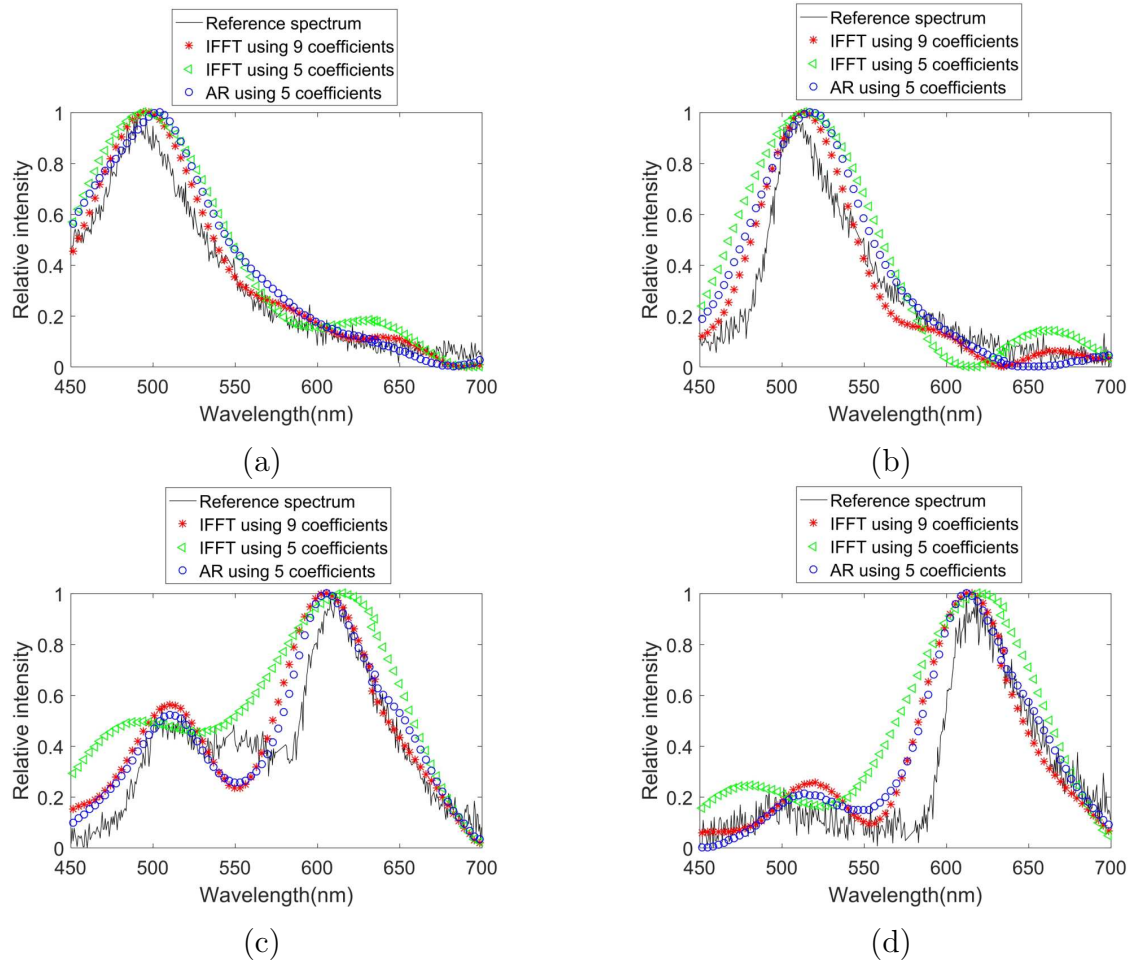


FIGURE 11. Comparison of the reference spectral curves measured by a commercial spectrometer and the reconstructed spectral curves using IFFT with 9 and 5 Fourier coefficients, AR method with 5 coefficients respectively, (a) blue digital 1; (b) green digital 2; (c) orange digital 4; (d) red digital 5

- [6] X. Sun, B. L. Hu, L. B. Li, and Z. H. Wang, An engineering prototype of Hadamard transform spectral imager based on digital micro-mirror device, *Optics and Laser Technology*, vol.44, pp.210-217, 2012.
- [7] K. Hirakawa, Fourier multispectral Imaging: measuring spectra, one sinusoid at a time, *CCIW 2017: Lecture Notes in Computer Science*, vol.10213, pp.3-12, 2017.
- [8] J. Jia, C. Ni, A. Sarangan, and K. Hirakawa, Fourier multispectral imaging, *Opt. Express*, vol.23, no.7, pp.22649-22657, 2015.
- [9] D. Dan, M. Lei, B. L. Yao, W. Wang, M. Winterhalder, A. Zumbusch, Y. J. Qi, L. Xia, S. H. Yan, Y. L. Yang, P. Gao, T. Ye, and W. Zhao, DMD-based LED-illumination super-resolution and optical sectioning microscopy, *Scientific Reports*, vol.3, no.1116, pp.1-7, 2013.
- [10] Z. B. Zhang, X. Ma, and J. G. Zhong, Single-pixel imaging by means of Fourier spectrum acquisition, *Nature Communications*, vol.6, no.6225, pp.1-6, 2015.
- [11] C. Ma, H. Lin, G. D. Zhang, and R. Du, Digital micro-mirror device based multispectral imaging using compressed Fourier spectrum, *Optics Communications*, vol.426, pp.348-358, 2018.
- [12] G. Han, X. B. Liu, B. L. Hu, and C. L. Wang, Interferogram spectrum reconstruction using modern spectral estimation, *IEEE*, pp.2112-2115, 2011.
- [13] Mutispectral Image Database: <http://www.cs.columbia.edu/CAVE/databases/multispectral/>